Applied Energy 261 (2020) 114361

Contents lists available at ScienceDirect

Applied Energy

journal homepage: www.elsevier.com/locate/apenergy

Underground solar energy storage via energy piles

Qijie Ma*, Peijun Wang

School of Civil Engineering, Shandong University, Jinan, Shandong, 250061, China

HIGHLIGHTS

- The thermal performance of energy piles for underground solar energy storage was investigated.
- A lower flow rate of the circulating water was preferred.
- The maximum daily average rate of solar energy storage reached 150 W/m.
- Thermal interference induced a 10 W/m reduction in the daily average rate of solar energy storage.

ARTICLE INFO

Keywords:
Energy pile
Solar energy storage
Ground source heat pump system
Thermal interference

ABSTRACT

Conventional piles embedded with geothermal loops, referred to as energy piles, have been successfully used as heat exchangers for the ground source heat pump system. For heating-dominated regions, it is crucial for the ground source heat pump system to keep the ground thermal balance in the long run. Solar energy is the most feasible source to charge the ground manually. In this study, thermal performance of an energy pile-solar collector coupled system for underground solar energy storage was investigated using numerical modeling. The results suggested that a lower flow rate should be adopted for the energy pile-solar collector coupled system to save the operational cost of the circulation pump. For the case with a pile length of 30 m, the decrease in the rate of solar energy storage was about 2% when the mass flow rate was reduced from 0.3 to 0.05 kg/s. Throughout a year, the maximum daily average rate of solar energy storage reached 150 W/m. It was also found that to increase the length and the diameter of the pile improved the thermal performance of the system by keeping its temperature relatively lower. In addition, the effects of the pile-pile thermal interference on reducing the rate of solar energy storage after a one-year operation were quantified to be within 10 W/m for groups with the pile-pile spacing of 3 times the pile diameter.

1. Introduction

According to the International Energy Agency, buildings are responsible for almost 40% of total final energy consumption in the European Union, out of which 80% is due to the heat demand, accounting for 30% of the total CO_2 emissions [1]. To reduce the carbon footprint and promote sustainable development, clean solar energy offers excellent potential for heat production to meet the demands of space heating in winter and domestic hot water production. Nevertheless, solar radiation varies daily and seasonally and is not constantly present. To cover the intermittency of the solar radiation, thermal energy storage is necessary so that heat can be extracted when the solar radiation is not available [2,3]. Based on the medium adopted, thermal energy storage can be classified as sensible, latent, and chemical heat storage. Of the common sensible mediums for thermal energy storage, the ground enjoys the advantage of enormous quantity and being widely accessible [4,5]. The conventional practice of underground thermal energy storage is burying heat exchange pipes into pre-drilled vertical holes, referred to as the borehole thermal energy storage [6]. Heat transfer occurs by circulating heat carrier fluid through the pipes. However, the cost of drilling deep holes can cause a breakdown of a project [4]. In addition, with the quick development of urbanization, the available free lands for drilling holes become increasingly more scarce and costly in cities. Both factors impede the application of the borehole thermal energy storage technology.

In recent years, energy piles have been attracting attention from the academic field and getting more installations in engineering practice [7–9]. The energy piles combine the foundation piles with the heat exchange pipes, the latter being attached to the steel cage and embedded in the pile body, as illustrated in Fig. 1. In this way, the energy

* Corresponding author.
E-mail address: qmaah@connect.ust.hk (Q. Ma).

https://doi.org/10.1016/j.apenergy.2019.114361
Received 4 September 2019; Received in revised form 28 November 2019; Accepted 10 December 2019

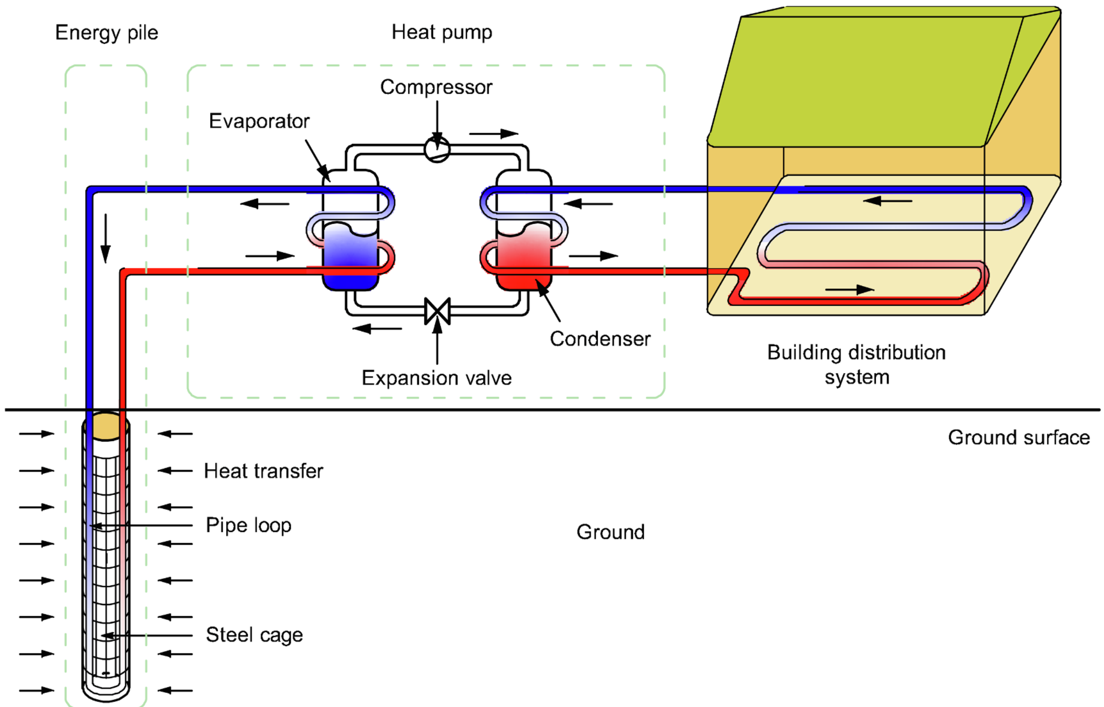

Fig. 1. Schematic diagram of the GSHP system coupled with energy pile (Modified from Sani et al. [9]).

piles sustain the building load and hold the heat exchange pipes simultaneously. Therefore, the underground space and the cost related to drilling additional boreholes can be saved. In addition, the concrete energy piles enjoy relatively larger thermal conductivity and heat storage capacity compared to the conventional boreholes [10]. The thermal performance of energy piles has been tested with manually controlled inlet temperature or heat flux rate under different operation modes (e.g., [11–13]). Zhao et al. [14] compared the effects of the pipe configuration and the spiral-shaped configuration was found to perform better than others. Park et al. [15] found that as the number of heat exchange pipes increases, the contribution to improving the thermal performance of energy piles gradually decreases due to the thermal interference between them. A novel truncated cone helix configuration was proposed and studied by Huang et al. [16] and Liu et al. [17] to reduce the thermal interference between pipes. Faizal et al. [18] gave a comprehensive review of the available ways to improve the thermal performance of energy piles. Li & Lai [19] reviewed the available analytical models for the thermal analysis of energy piles. Recently, Liu et al. [20] and Kong et al. [21] demonstrated the feasibility of energy piles for bridge snow melting.

The energy piles have been successfully used in the ground source heat pump (GSHP) system to replace the traditional boreholes (see Fig. 1). The GSHP system uses the ground as a heat source or a heat sink. Heat is injected into the ground in summer and extracted from it in winter. It takes advantage of the relatively constant ground temperature throughout the year about 10 m below the ground surface. Therefore, it outperforms the air source heat pump system. A coefficient of performance close to 4.0 was reported for the GSHP system coupled with energy piles [22]. For the GSHP system, however, it is critical to keep the ground thermal balance to achieve a long-term high performance [21,24]. For heating-dominated areas, the natural recovery is usually not enough to meet the continuous heat extraction in winter, resulting in ground thermal imbalance and gradually decreasing heat exchange rate in the long run. The solar-assisted GSHP system has therefore been suggested to maintain the ground thermal balance [25–28]. As a successful application, over 90% of the heat demand was provided by the solar energy in the Drake Landing project, which employs 144 boreholes with a depth of 37 m [29].

The novelty of this study lies in the proposed energy pile-solar collector coupled system, the thermal performance of which for underground solar energy storage has not been studied yet. There are two main different features of the energy pile-solar collector coupled system compared to the traditional borehole system for underground thermal energy storage. First, the concrete pile material and the larger pile diameter help to improve the thermal performance of energy piles. Nevertheless, the energy piles are relatively shorter, usually less than 50 m. This leads to a smaller storage volume for each single energy pile. It should also be always borne in mind that the primary function of the energy piles is to support the structures built upon it. Therefore, the temperature changes of the energy piles should be kept within a safe value to ensure that thermal effects on its geotechnical performance are acceptable [30,31].

In this study, a mathematical model for the energy pile-solar collector coupled system was developed first and validated against field test results on energy piles. The model was built based on the component approach, and the components were coupled through the heat transfer between them. A systematic parametric study adopting steady-state analysis was then conducted to evaluate the effects of different system parameters, including the flow conditions, the characteristics of the solar collector, the intensity of solar radiation, the ambient air temperature, and the ground conditions. From the parametric study, major factors affecting the thermal performance of the energy pile-solar collector coupled system for underground solar energy storage were identified. In addition to the steady-state analysis, transient-state simulations were also performed to study the evolution with time of the thermal performance of the energy pile-solar collector coupled system. The focus was put on the rate of underground solar energy storage and the temperature change of the system. The effects of the pile length, the pile diameter, and the pile-pile thermal interaction were evaluated in the transient-state analysis.

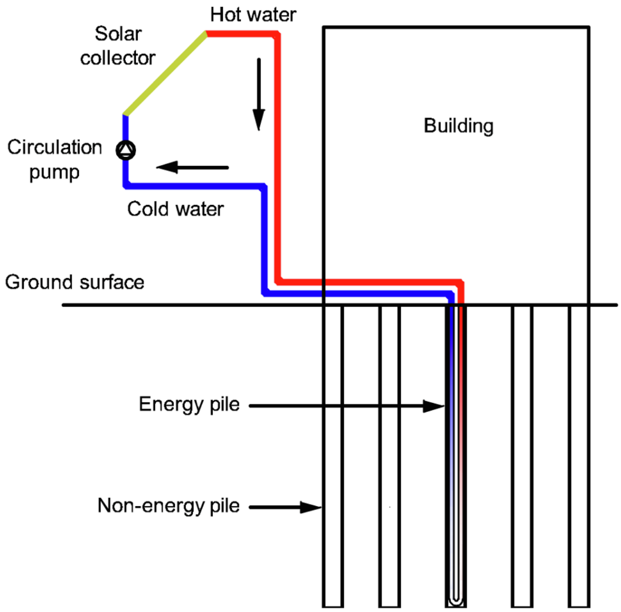

Fig. 2. Schematic diagram of the energy pile-solar collector coupled system for underground solar energy storage.

2. Methodology

2.1. Mathematical formulation

Fig. 2 shows a schematic diagram of the energy pile-solar collector coupled system to be modeled in this study. It consists of a flat-plate solar collector, an energy pile with the surrounding soil, and the water-bearing pipes. The building upon the pile foundation is also shown in the figure, but not modeled. The effect of the building on the thermal performance of the system was accounted for by setting a constant-temperature boundary condition at the top ground surface of the model domain. Both single energy piles and energy pile groups considering the potential pile-pile thermal interference were modeled in this study. For the energy pile groups, the same independent flat-plate solar collector was connected to each energy pile of the group.

According to Duffie & Beckman [32], the flat-plate solar collector was modeled using the following equation:

$$q_u^{'} = w{\cdot}F^{'}{\cdot}[(\tau\alpha{\cdot}G_T) - U{\cdot}(T_f - T_a)] \tag{1}$$

where $q_u^{'}$ is the useful energy gain of the circulating water per unit length of the solar collector tube; w is the tube spacing of the solar collector; F' is the collector efficiency factor; $\tau\alpha$ is the transmittance-absorptance product; G_T is the total available solar irradiation; U is the overall heat loss coefficient to the ambient; T_f and T_a are the fluid temperature and the ambient air temperature, respectively. For all the analyses conducted in this study, typical values of the tube spacing (0.15 m), the collector efficiency factor (0.9), and the transmittance-absorptance product (0.75) were adopted.

Heat transfer through the ground (soil in this study) can include all the three modes conduction, convection, and radiation, with the conduction dominating most cases when the groundwater flow is negligible [7]. It should be noted that the convective heat transfer due to groundwater flow can cause opposite effects on the thermal performance of the underground solar energy storage system and the GSHP system. For the underground solar energy storage system, the groundwater flow can increase the heat loss due to self-discharge [33], while for the latter it facilitates the heat restoration [34]. In this study, only the thermal conduction was considered for the heat transfer through the soil. This assumption is reasonable considering that the dry soil condition was adopted for most analyses conducted in this study. The three phases of the soil were assumed being at local equilibrium, implying the same temperature for them. Accordingly, the following three-dimensional heat diffusion equation was solved for the soil and also the concrete energy pile, assuming they share the same temperature at the pile-soil interface:

$$\rho c_p(\partial T/\partial t) - \nabla{\cdot}(k\nabla T) - q = 0 \tag{2}$$

where T is the temperature; t is the time; q is the heat source term; ρ, k, and c_p are the density, thermal conductivity, and specific heat capacity of the materials, respectively.

Density, thermal conductivity, and specific heat capacity of a soil are functions of its void ratio (e) and degree of saturation (S_r). According to Johansen [35] and Brandl [7], they can be related through the following equations:

$$\rho_{soil} = (G_s + S_r e){\cdot}\rho_{water}/(1 + e) \tag{3}$$

$$k_{soil} = \prod (k_i)^{x_i} \tag{4}$$

$$(c_p)_{soil} = \sum c_i x_i \tag{5}$$

where G_s is the specific weight of the soil particles with a typical value of 2.65; x_i is the specific volume of each phase of the soil: $x_w = nS_r$ for the water phase, $x_a = n(1 - S_r)$ for the air phase, and $x_s = 1 - n$ for the solid phase, where $n = e/(1 + e)$ is the soil porosity. The adopted thermal properties of the water, air, and soil particles are listed in Table 1 [7,36]. The typical thermal properties of the concrete pile are based on the European design code [37].

The water circulation through the pipes was modeled using the following one-dimensional convection-diffusion heat transfer equation:

$$\rho c_p\left(\frac{\partial T}{\partial t} + v{\cdot}\frac{\partial T}{\partial s}\right) - \frac{\partial}{\partial s}{\cdot}\left(k{\cdot}\frac{\partial T}{\partial s}\right) - q = 0 \tag{6}$$

where v is the velocity of the circulating water; s is the distance along the flow path. When the thermal conduction term is dropped ($k = 0$), Eq. (6) is close to the further simplification adopted by Park et al. [38]. To ignore the thermal conduction term is reasonable when the heat transport by convection dominates over that by conduction for turbulent conditions. In this study, the complete form of Eq. (6) was solved, considering that a wide range of flow velocity was simulated.

Eq. (1) serves to determine the heat source term (q) of Eq. (6) when the water passes through the solar collector. The coupling between Eq. (2) and Eq. (6) is also realized via the heat source term (q) when the water passes through the pipes embedded in the energy pile. The amount of heat transfer (q) between the circulating water and the energy pile is calculated by:

$$q = h_f{\cdot}(T_f - T_p) \tag{7}$$

where T_f and T_p are the temperature of the circulating water and the adjacent energy pile, respectively. h_f is the convective heat transfer coefficient between them. It was estimated using the Dittus-Boelter correlation:

$$h_f = 0.023{R_e}^{0.8}{P_r}^n\frac{k_f}{D} \tag{8}$$

where k_f, R_e, and P_r are the thermal conductivity, the Reynolds number, and the Prandtl number of the circulating fluid, respectively. D is the

Table 1
Thermal properties of different materials adopted in this study.

Material	Density (kg/m^3)	Thermal conductivity (W/m/°C)	Heat capacity (J/kg/°C)
Water	1000	0.57	4200
Air	1.25	0.026	1000
Soil particles	2650	4.0	1000
Concrete	2500	1.6	900

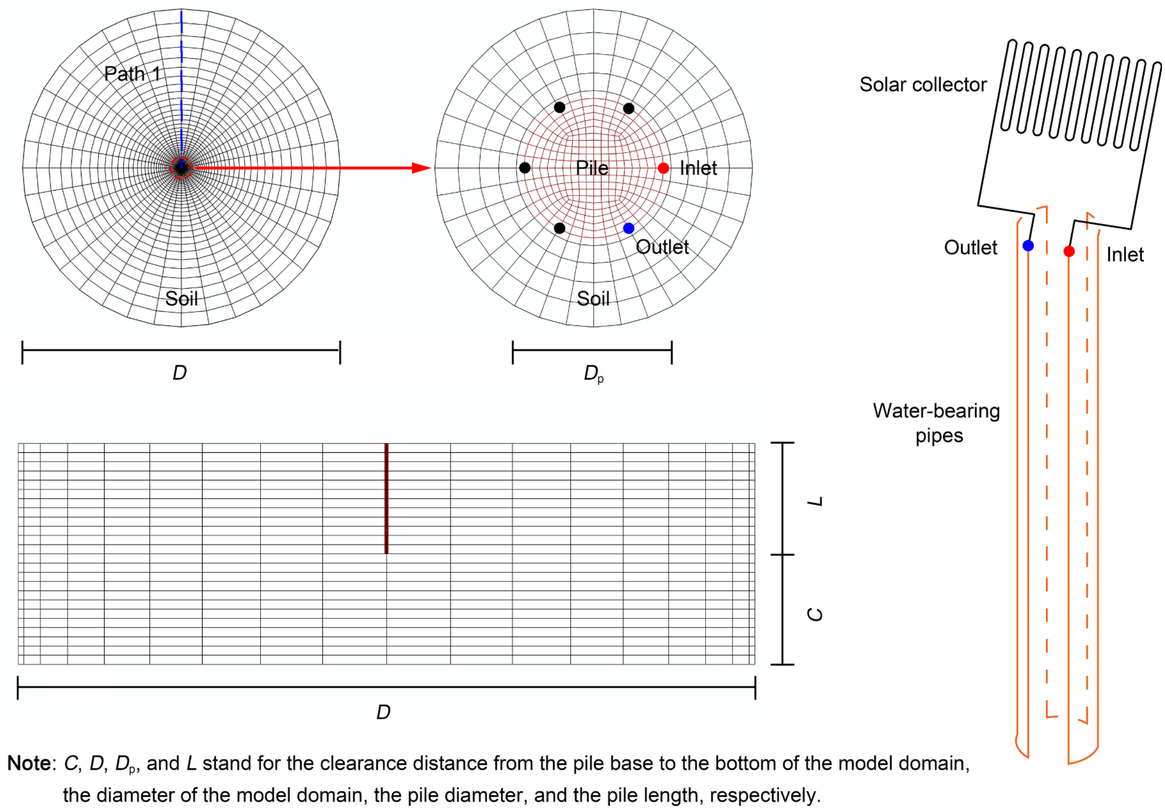

Fig. 3. Dimensions and mesh of the model domain for a single energy pile-solar collector coupled system.

inside diameter of the pipe. $n = 0.4$ for heating ($T_f > T_p$) and $n = 0.3$ for cooling ($T_f < T_p$). Although the water-bearing pipe was not modeled directly in this study, its effects on the thermal performance of the system were evaluated as to be discussed later in Section 3.1.

2.2. Numerical implementation

The above developed mathematical model was solved using the finite element software Abaqus/Standard [39]. A typical finite element mesh of the model domain for a single energy pile-solar collector coupled system is shown in Fig. 3. Typical dimensions were chosen for the simulated energy pile and the embedded water-bearing pipes according to Bozis et al. [40]. The water-bearing pipes were taken to have an inside diameter of 0.02 m. The distance from the center of the pipe to the periphery of the pile was taken to be 0.05 m. The concrete pile and the ground were modeled using three-dimensional diffusive heat transfer elements DC3D8. The 3U-in-series shaped water-bearing pipes embedded within the pile body was modeled using the one-dimensional forced convection heat transfer elements DCC1D2. The mesh of the pile and the adjacent ground region was particularly refined to capture their relatively large temperature gradients. The mesh of the water-bearing pipes was manually numbered in an ascending order along the flow direction. The inlet and outlet of the water circulation denoted in the figure are defined with respect to the energy pile. The heat transfer between the circulating water and the surrounding concrete pile was modeled using thermal contact with a flow velocity-dependent heat

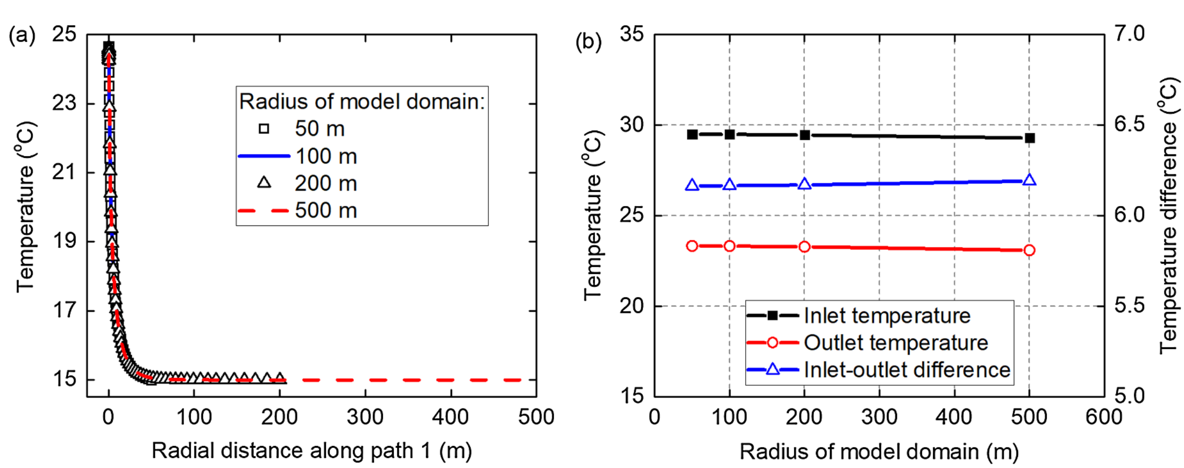

Fig. 4. Effects of the radius of the model domain on: (a) temperature distribution along the radial direction; (b) inlet, outlet temperature and their difference.

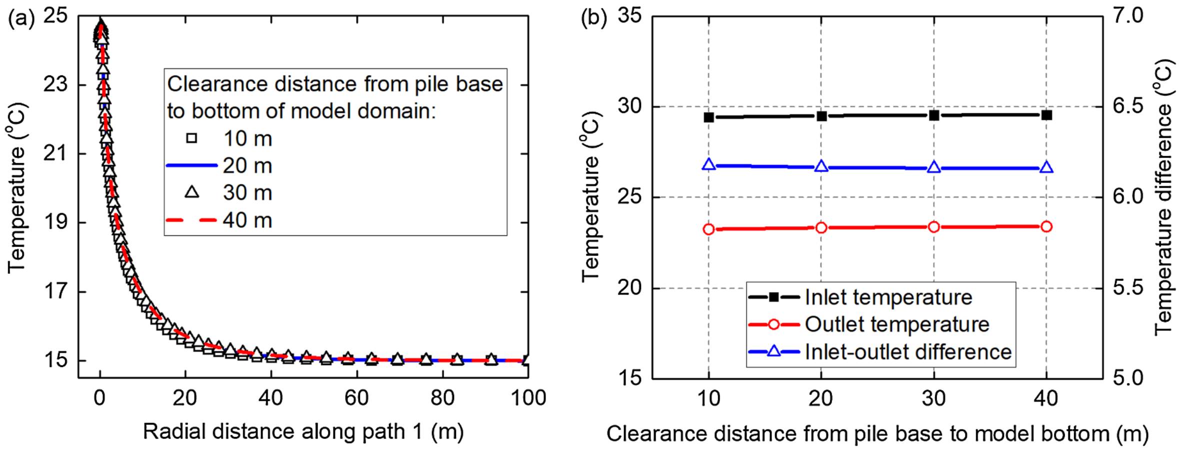

Fig. 5. Effects of the clearance distance from the pile base to the bottom of the model domain on: (a) temperature distribution along the radial direction; (b) inlet, outlet temperature and their difference.

transfer coefficient. The pile-soil interface was modeled using common nodes, assuming they share the same temperature. The heat transfer with the ambient air when the water passes through the solar collector was realized by setting two thermal boundary conditions. One is a concentrated heat flux boundary condition corresponding to the first term of Eq. (1). The other is a thermal contact boundary condition corresponding to the second term of Eq. (1).

The initial temperature of the whole domain was assumed to be at 15 °C, as adopted by Bourne-Webb et al. [41]. Constant-temperature boundary conditions were set at the outer lateral and the bottom surface of the model domain. To fulfill this assumption, the model domain should be large enough so that the assumed boundary conditions have negligible effects on the results. This was achieved by carrying out a sensitivity analysis to determine the dimensions of the model domain.

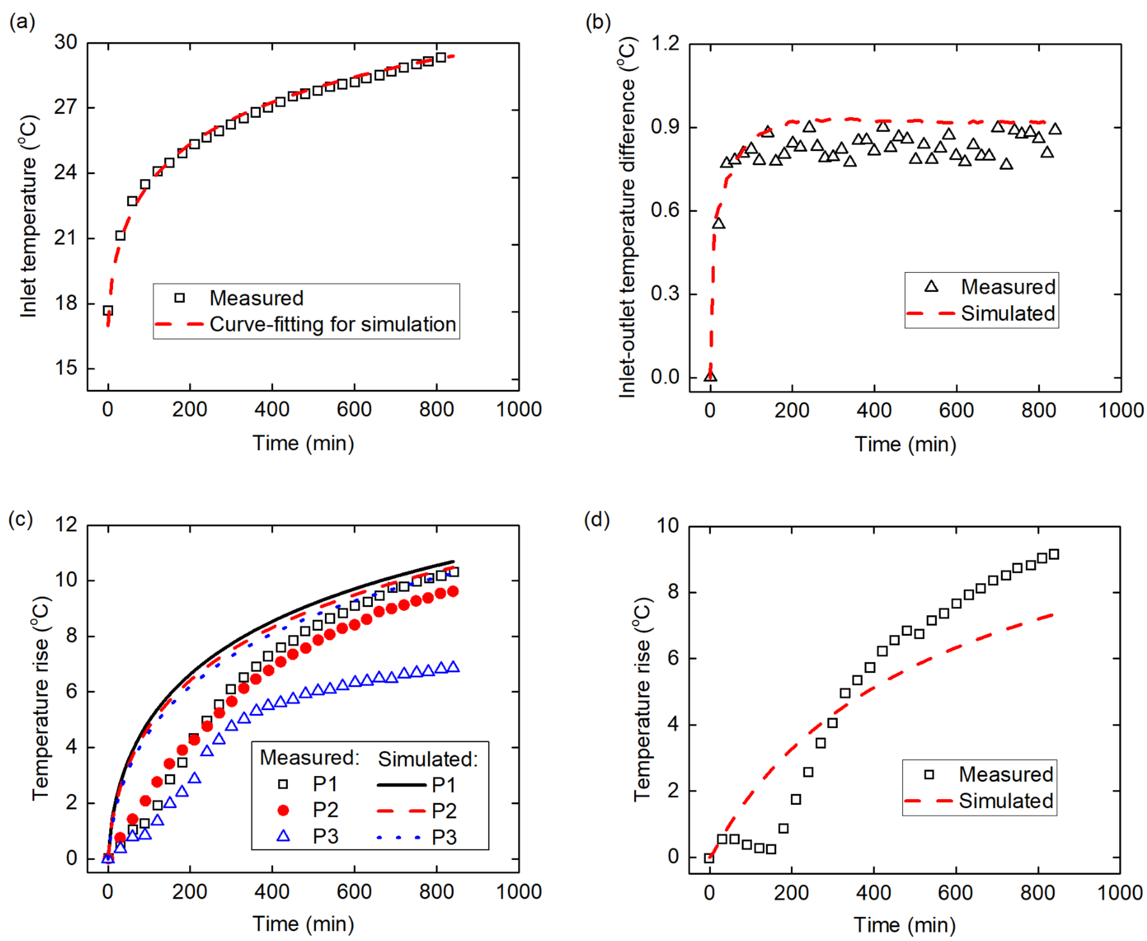

Fig. 6. Validation of the developed model: (a) inlet temperature; (b) inlet-outlet temperature difference; (c) pipe temperature at different locations along the flow path; (d) concrete temperature.

Table 2
Details of the parametric study.

Series No.	Number of energy piles	Analysis type	Mass flow rate (kg/s)	Convective heat transfer coefficient (W/m^2/°C)	Overall loss coefficient (W/m^2/°C)	Air temperature (°C)	Solar irradiance (W/m^2)	Length of solar collector tube (m)	Void ratio of soil	Degree of saturation of soil (%)	Pile length (m)	Pile diameter (m)
1	Single pile	Steady-state	From 0.05 to 0.3	From 100 to 1000	6	15	600	20	0.7	0	30	1.0
2			0.05	Eq. (8)	From 1 to 10	From 15 to 35						
3					6	15	From 100 to 650	From 10 to 50				
4							600	20	From 0.6 to 0.9	From 0 to 100%		
5		Transient-state				Time variations (Fig. 13)			0.7	0	From 10 to 50	
6											30	From 0.5 to 1.5
7	2 × 2 & 3 × 3 Pile group											1.0

Based on the results from the sensitivity analysis (see Figs. 4 & 5), the radius and the clearance distance from the pile base to the bottom of the model domain were determined to be 100 m and 10 m, respectively. From Fig. 4(a) it can be seen that the soil temperature corresponding to the steady-state is not affected when the radial distance reaches about 100 m. Fig. 4(b) shows that the radius of the model domain has almost no effects on the steady-state inlet-outlet temperature difference, which represents the rate of solar energy storage. Fig. 5 demonstrates that the effects of the clearance distance from the pile base to the bottom of the model domain are negligible after it exceeds 10 m. A constant-temperature condition was also set at the top surface of the model domain. This is based on the consideration that the top surface is covered by the building, and its basement temperature can be assumed to be maintained constant throughout the year [41].

2.3. Model validation

The above-developed model was validated against the field test on a single energy pile conducted by Park et al. [38]. For the field test, there was no solar collector, and the input heat flux was controlled manually. In addition, the top ground surface was insulated so that a no-heat-flux boundary condition, instead of a constant-temperature boundary condition, was adopted in the model validation. The geometrical dimensions and material properties used in the model validation followed the details provided by Park et al. [38]. The measured variations of the inlet temperature (see Fig. 6(a)) were curve-fitted and used as the input in the model validation. It should be noted that the solar collector was not considered in the model validation. Nevertheless, the mathematical equation adopted to describe the performance of the solar collector was well developed and widely used [32]. The practical issue lies in determining the parameters characterizing the specific solar collector of interest.

The simulated outlet temperature, pipe temperature at different locations along the flow path, and the concrete temperature are compared to the measured values in Fig. 6(b–d). It should be noted that grout was used in the original publication. Concrete is used here to be consistent with other sections. Overall, they show a reasonably good agreement with each other. Regarding the inlet-outlet temperature difference, the simulated results show a slightly higher value after it turns to be almost constant, as shown in Fig. 6(b). The pipe temperature decreases gradually in the flow direction (from P1 to P3) due to continuous heat loss to the surrounding concrete. The numerical simulation reproduces the same trend. Quantitatively, it overestimates the pipe temperature, particularly for the third point P3, with a maximum difference of about 4 °C. It should be noted that the measured temperature drop from P2 to P3 is more significant compared to that from P1 to P2. This is not as anticipated considering that the distance between them is the same. The temperature drop from P2 to P3 should be smaller due to the continuously decreased temperature gradient between the circulating water and the surrounding concrete. In reality, it is likely that the non-uniform soil properties and other unidentified factors lead to the observed larger temperature drop from P2 to P3. Fig. 6(d) indicates that the simulated evolution of the concrete temperature correlates well with the measured results with a maximum difference of about 2 °C.

2.4. Numerical program

Both steady-state and transient-state heat transfer analyses were conducted in this study. The steady-state analysis was to evaluate the effects of different parameters on the thermal performance of the system. For each steady-state simulation, the solar irradiation and the ambient air temperature were kept constant. The transient-state analysis was to study the evolution of the thermal performance of the system with time-varying solar irradiation and ambient air temperature through a year. The parameters studied are summarized in Table 2. For most cases, the dry soil condition was used. This is based on the

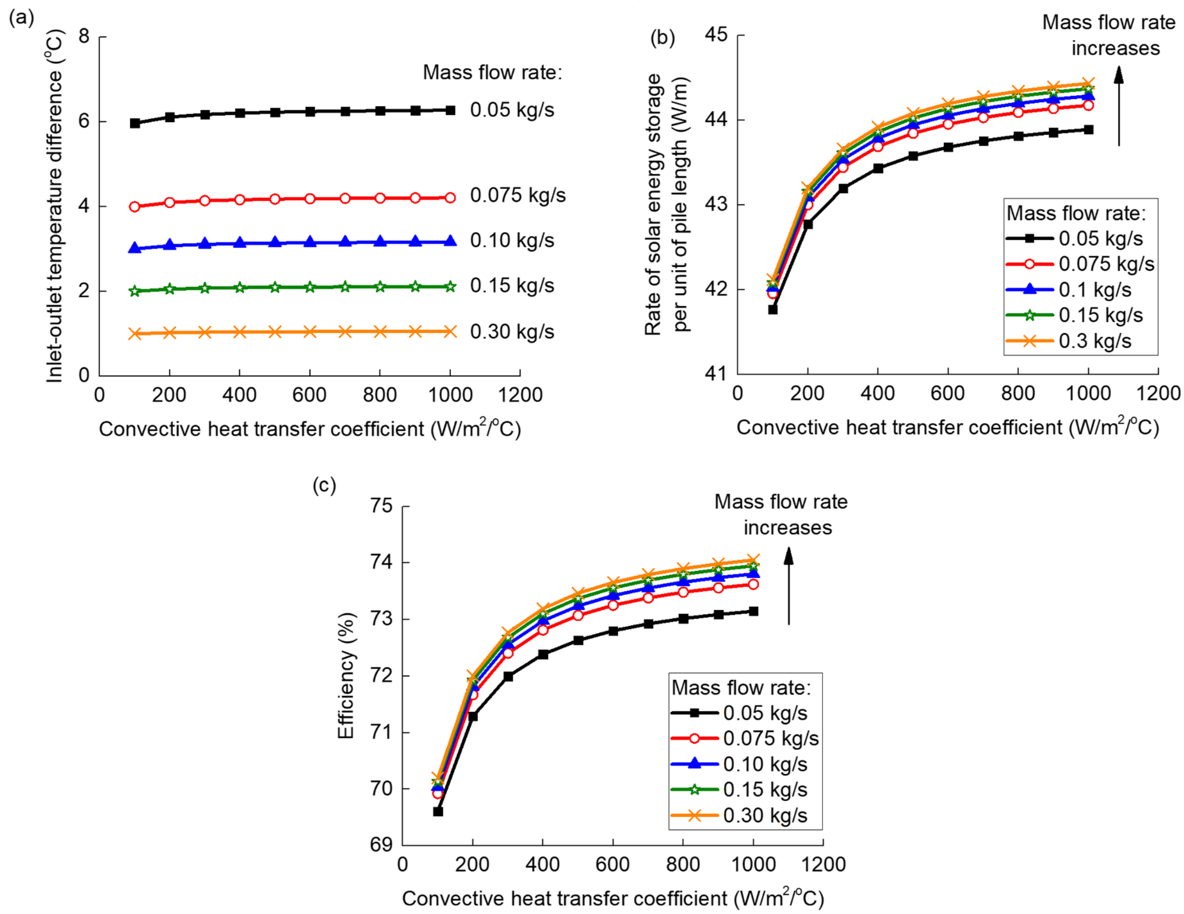

Fig. 7. Effects of the convective heat transfer coefficient and the mass flow rate on: (a) inlet-outlet temperature difference; (b) rate of solar energy storage; (c) system efficiency.

consideration that due to its relatively low thermal conductivity and small heat capacity, results corresponding to the dry soil condition should represent the worst case in terms of the thermal performance of the system. In addition, during underground solar energy storage, temperature increase drives the moisture away from the storage zone [42]. Correspondingly, a dry soil condition is usually assumed in the pure conduction analysis [4].

3. Steady-state analysis

In the following interpretation of the numerical results, the focus is put on the inlet-outlet temperature difference ($T_{in} - T_{out}$), the rate of solar energy storage per unit of pile length (q_{sto}/L), and the efficiency of the system (η). The rate of solar energy storage q_{sto} and the system efficiency η are calculated as follows:

$$q_{sto} = \dot{m}c_w(T_{in} - T_{out}) \tag{9}$$

$$\eta = q_{sto}/(F^{'}\cdot\tau\alpha G_T\cdot wl) \tag{10}$$

where $\dot{m}$ is the mass flow rate; c_w is the specific heat capacity of water; T_{in} and T_{out} are the inlet and outlet temperature of the circulating water (see Fig. 3), respectively. $F^{'}\tau\alpha G_T$ is the absorbed solar energy by the circulating water per area of the solar collector. w and l are the spacing and the length of the solar collector tube, respectively. Essentially, the efficiency defined here characterizes the relative proportion between the solar energy injected into the ground and that lost to the air as the water passes through the solar collector.

The steady-state analysis was conducted to study the sensitivity of the thermal performance of the energy pile-solar collector coupled system to different parameters. The rate of solar energy storage corresponding to the steady-state is supposed to be at the lowest level due to the gradual increase in the ground temperature. In addition, corresponding to the steady-state, there is no change in the temperature of the system, indicating that the model domain has been fully charged. Therefore, the rate of solar energy storage corresponding to the steady-state also equals that of the energy loss to the building and the ground outside the model domain.

3.1. Effects of the convective heat transfer coefficient and the mass flow rate

The convective heat transfer coefficient between the circulating water and the surrounding concrete pile depends on the flow rate of the water and the characteristics of the water-bearing pipes. To model it accurately, an equivalent heat transfer coefficient should be adopted, accounting for the thickness and the thermal conductivity of the pipe [38]. In this study, the effects of the water-bearing pipes were evaluated by keeping the mass flow rate constant and changing the convective heat transfer coefficient. Fig. 7 shows its effects on the thermal performance of the system for 5 different mass flow rates. It is expected that the temperature drop of the circulating water from the inlet to the outlet increases with the convective heat transfer coefficient. This is observable as the convective heat transfer coefficient increases from 100 to about 600 W/m^2/°C, particularly for smaller mass flow rates, as shown in Fig. 7(a). With a further increase in the convective heat transfer coefficient, its contribution is almost negligible. Compared to the convective heat transfer coefficient, the temperature drop is more sensitive to the mass flow rate. Fig. 7(a) shows that it increases from about 1 to 6 °C as the mass flow rate decreases from 0.3 to 0.05 kg/s.

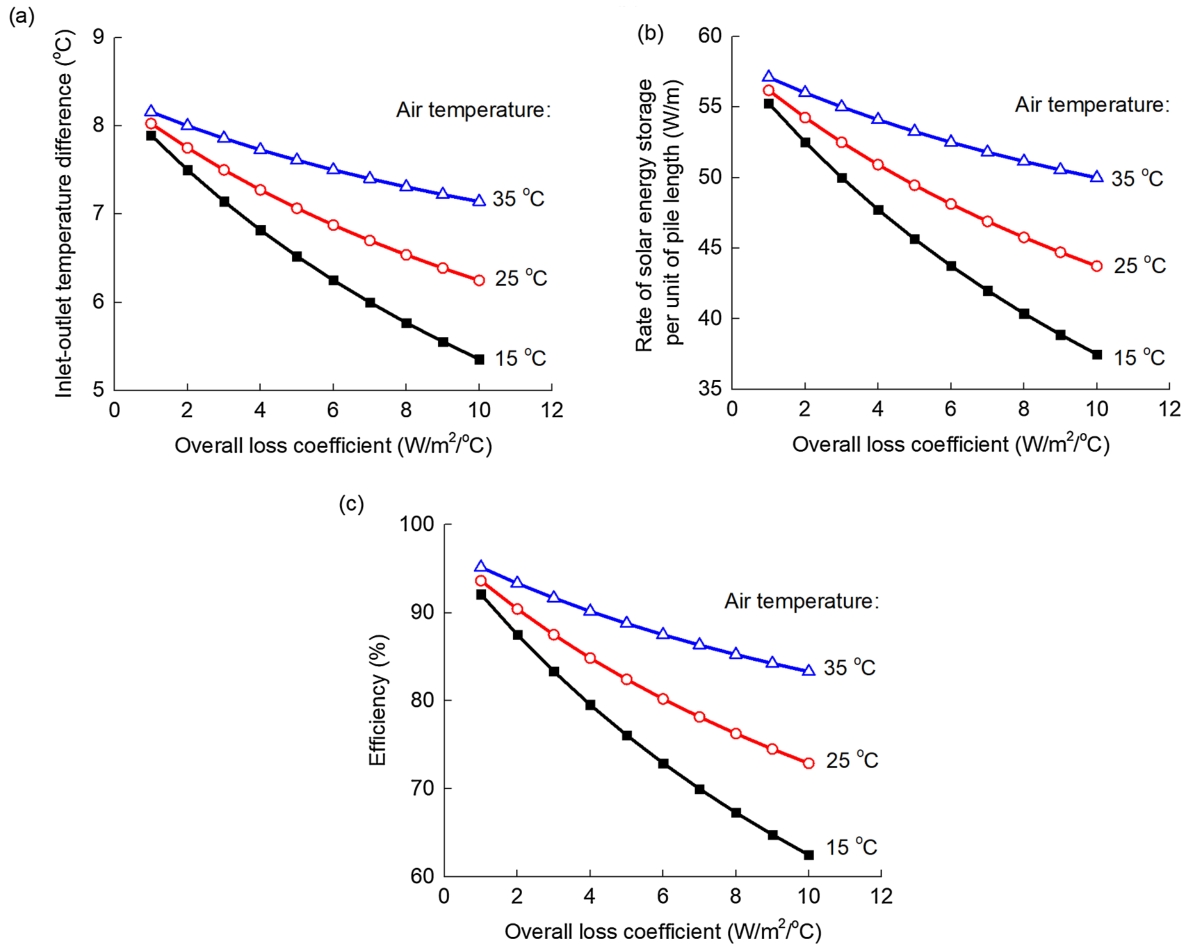

Fig. 8. Effects of the air temperature and the overall loss coefficient on: (a) inlet-outlet temperature difference; (b) rate of solar energy storage; (c) system efficiency.

This is because a smaller mass flow rate allows more time for the heat transfer between the circulating water and the surrounding pile. The same trend was also observed by Gao et al. [8] and Başer et al. [43].

Both a larger convective heat transfer coefficient and a higher mass flow rate contribute to increasing the rate of solar energy storage, as shown in Fig. 7(b), being consistent with the experimental findings from Jalaluddin et al. [44]. While the increase is quite small, less than 3 W/m, as the convective heat transfer coefficient increases to 1000 W/m^2/°C. When the energy pile serves as a heat exchanger for the GSHP system, the mass flow rate is usually about 0.25 kg/s to create a turbulent flow condition and increase the convective heat transfer coefficient [45]. When used for underground solar energy storage, the results suggest that the mass flow rate should be reduced to save the operational cost of the circulation pump. This only causes a slight sacrifice of the rate of solar energy storage, less than 2%, as the mass flow rate is reduced from 0.3 to 0.05 kg/s. Therefore, a mass flow rate of 0.05 kg/s was used for the remaining analyses of this study. This is close to the mass flow rate (0.09 kg/s) for the heat injection test adopted by Zarrella et al. [46]. For the remaining analyses, the convective heat transfer coefficient was calculated using Eq. (8) directly without considering the effects of the water-bearing pipes as they are relatively small. Regarding the system efficiency, it is supposed to follow a similar pattern to the rate of solar energy storage as the intensity of solar radiation and the area of the solar collector are the same for the cases shown in Fig. 7. Overall, the system efficiency corresponding to the steady-state is more than 70%, as shown in Fig. 7(c). This means less than 30% of the solar energy absorbed by the circulating water was lost to the ambient air during its pass-through the solar collector.

3.2. *Effects of the air temperature and the overall loss coefficient of the solar collector*

As expressed in Eq. (1), the air temperature and the overall loss coefficient affect the heat transfer between the circulating water and the air during its flow through the solar collector. The amount of heat transfer depends linearly on the temperature difference between the circulating water and the ambient air. Therefore, it is expected that higher air temperature can promote solar energy storage by reducing the heat loss to the air, as demonstrated in Fig. 8(a). This is more evident for cases with larger overall loss coefficients. When the air temperature increases from 15 to 35 °C, the increase in the inlet-outlet temperature difference reaches about 2.5 °C for the cases with the overall loss coefficient $U = 10$ W/m^2/°C. Correspondingly, the rate of solar energy storage increases by about 15 W/m, as shown in Fig. 8(b). The rate of solar energy storage decreases with the increase of the overall loss coefficient due to more heat loss to the air. It drops more quickly when the air temperature is low. The minimum value is slightly more than 35 W/m. The system efficiency follows a similar pattern to that of the solar energy storage. When the overall loss coefficient is small, the system efficiency reaches 95%. For the worst condition, it drops to about 60%.

3.3. *Effects of the solar irradiance and the length of the solar collector tube*

The solar irradiance varies over time and locations, and it depends on the incidence angle and the climate conditions [32]. As the solar irradiance increases, a larger inlet-outlet temperature difference is

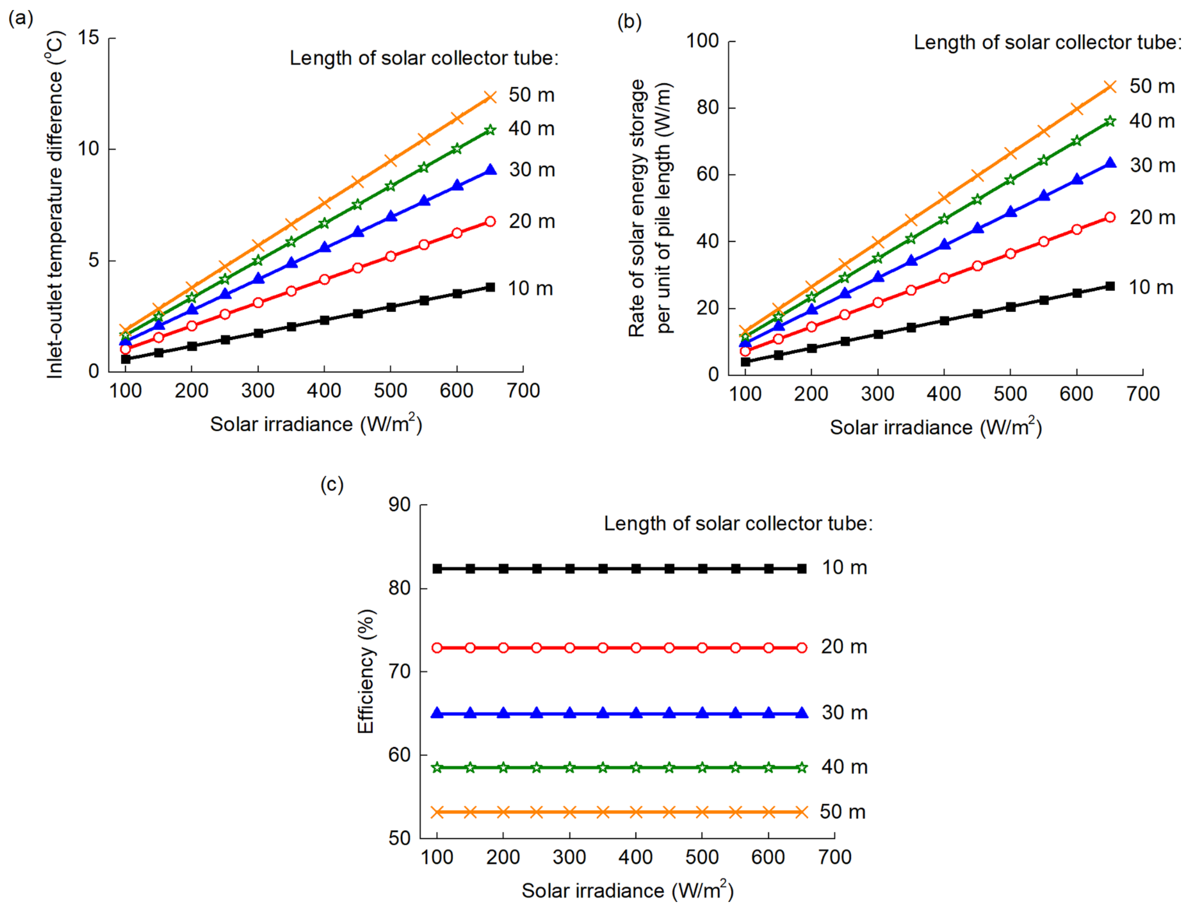

Fig. 9. Effects of the solar irradiance and the length of solar collector tube on: (a) inlet-outlet temperature difference; (b) rate of solar energy storage; (c) system efficiency.

expected since the circulating water absorbs more heat during its passthrough the solar collector. This is confirmed by the numerical results shown in Fig. 9(a). A larger inlet-outlet temperature difference corresponds to a higher rate of solar energy storage. Fig. 9(b) shows that for the case with the length of the solar tube l = 10 m, the rate of solar energy storage increases from slightly more than 0 to about 20 W/m when the solar irradiance increases from 100 to 650 W/m^2. This trend is even more significant for the case with l = 50 m. It increases from about 15 to almost 90 W/m.

Although an increase in the solar irradiance improves the rate of solar energy storage, it has almost no effect on the efficiency of the system, as shown in Fig. 9(c). This is because as the circulating water absorbs more heat, its temperature increase turns to be higher. Therefore, it loses more heat to the air for the simulated condition with

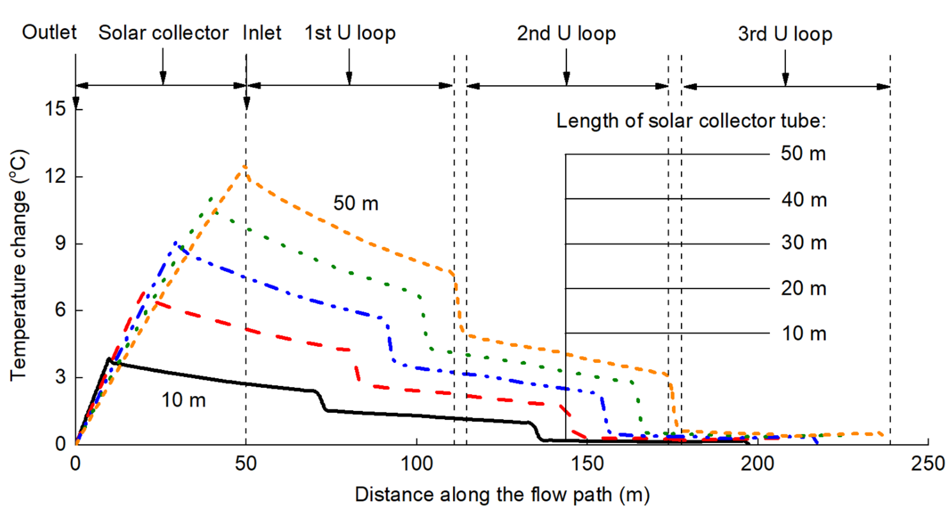

Fig. 10. Distribution of the circulating water temperature along its flow path for cases with different lengths of the solar collector tube.

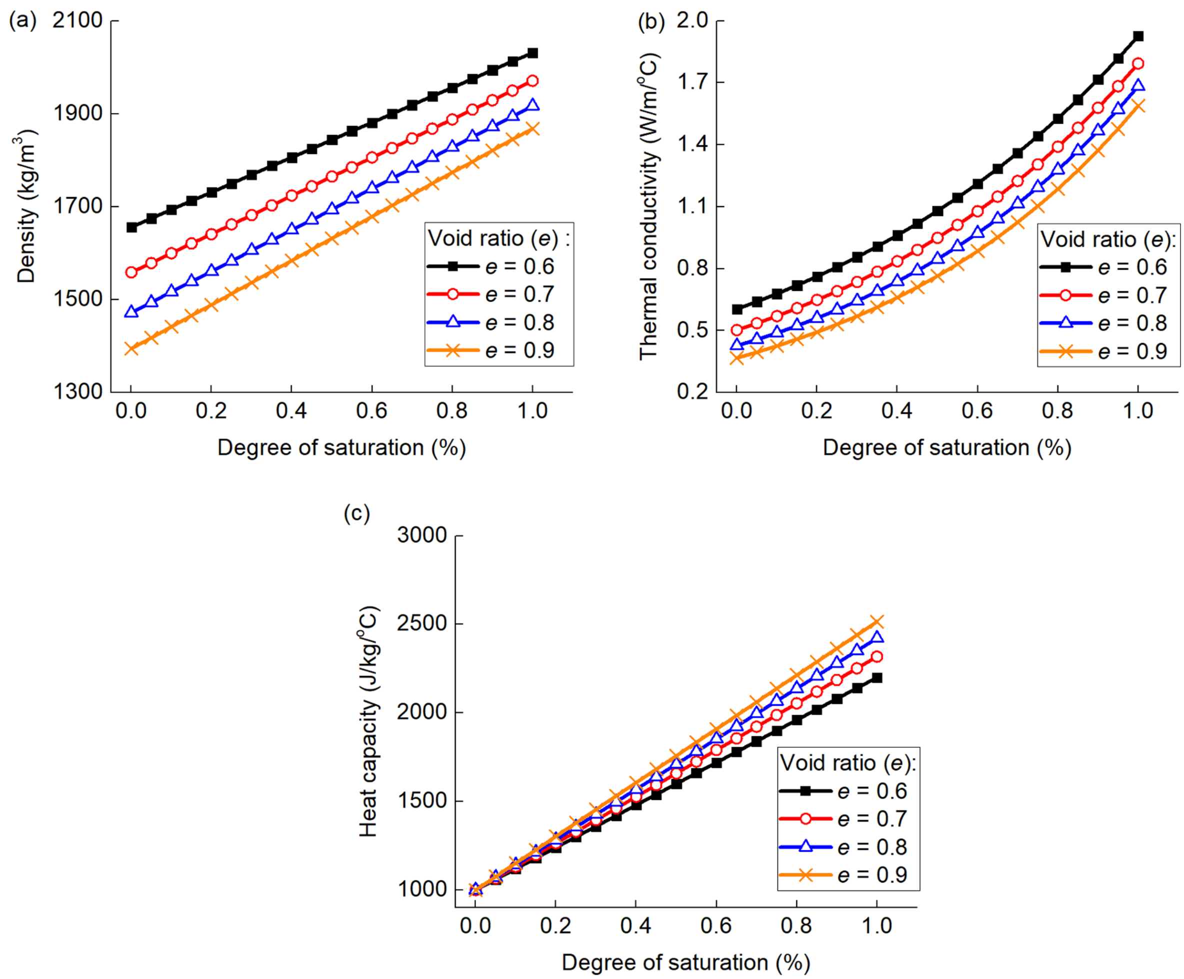

Fig. 11. Effects of the void ratio and the degree of saturation on soil properties: (a) density; (b) thermal conductivity; (c) specific heat capacity.

constant air temperature. Consequently, the system efficiency remains almost unchanged as it characterizes the relative proportion between the stored solar energy over that lost to the air. If the variations of the air temperature with the solar irradiation were considered, some non-linearity should then be observed. Nevertheless, the system efficiency decreases from about 80% to about 50% as the length of the solar collector tube increases from 10 to 50 m. This is because the temperature of the circulating water continues to increase as it flows through the solar collector. Therefore, as the length of the solar collector tube increases, the circulating water loses increasingly more heat to the air, and the efficiency of the system decreases accordingly.

The temperature distribution of the circulating water along its flow path is shown in Fig. 10 for cases with different lengths of the solar collector tube. It shows that during pass-through the solar collector, the temperature gradient of the water decreases as the length of the solar collector tube increases. This indicates more heat loss to the air, and thus a lower system efficiency. It can also be observed from Fig. 10 that the gradient of temperature drop during the three loops gradually decreases from the 1st loop to the 3rd loop. This is due to the continuous decrease of the water temperature. The part between the 1st and the 2nd U loop and that between the 2nd and the 3rd U loop are at the top of the energy pile. They are in direct contact with the basement of the building, the temperature of which was assumed to be a constant value of 15 °C. Therefore, the gradient of temperature drop along these two parts is relatively more significant.

3.4. Effects of the ground conditions

Both the void ratio and the degree of saturation have some effects on the soil thermal properties, including the density, the thermal conductivity, and the specific heat capacity [4]. Therefore, they can affect the thermal performance of the system. As demonstrated in Fig. 11, where the values are calculated using Eqs. (3)–(5), all three properties increase with the degree of saturation. Both the density and the thermal conductivity increase as the void ratio decreases. This is because the soil particles have larger values of density and thermal conductivity compared to the other two components (see Table 1). Nevertheless, the specific heat capacity decreases with the void ratio due to the smaller heat capacity of soil particles compared to that of water. This is more evident for cases with higher degrees of saturation, as shown in Fig. 11(c). The thermal properties of the soil studied here are within their typical ranges, as reported by Bozis et al. [40]. The density, the thermal conductivity, and the specific heat capacity range from 1400 to 2100 kg/m^3, from 0.3 to 2.0 W/m/°C, and from 1000 to 2500 J/kg/°C, respectively.

The resultant effects of the void ratio and the degree of saturation on the thermal performance of the energy pile-solar collector coupled system are shown in Fig. 12. Overall, as the degree of saturation increases, the thermal performance of the system improves remarkably. When the soil condition turns from being completely dry to being fully saturated, the rate of solar energy storage increases by about 10 W/m

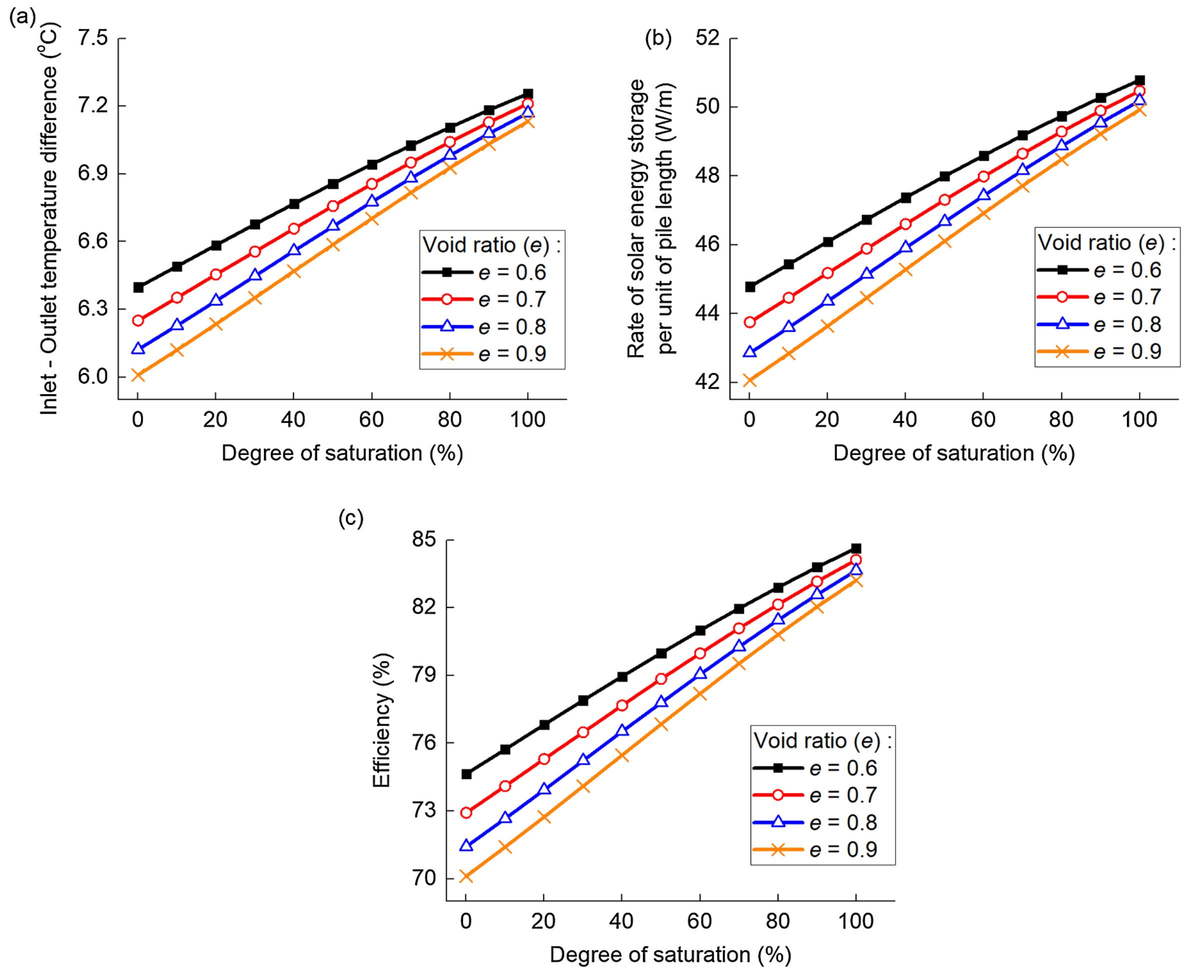

Fig. 12. Effects of the void ratio and the degree of saturation of soil on: (a) inlet-outlet temperature difference; (b) rate of solar energy storage; (c) system efficiency.

(20%), and the system efficiency also increases by about 10%. They are consistent with the results on the thermal performance of energy piles, as reported by Park et al. [45] and Akrouch et al. [47]. The reason lies in the degree-of-saturation-driven increase in the density, the thermal conductivity, and the specific heat capacity of the soil, as illustrated in Fig. 11. Compared to the degree of saturation, the void ratio has relatively smaller effects on the thermal performance of the system due to its limited effects on the soil thermal properties.

4. Transient-state analysis

A total of seven cases were analyzed to study the evolution of the thermal performance of the system with varying solar irradiance and ambient air temperature, as shown in Fig. 13. A time period of 12 months from Jan 01 to Dec 30 was simulated to consider the seasonal solar energy storage throughout a year. The adopted daily and hourly variations of the solar irradiance and the ambient air temperature were based on the climate conditions of Jinan, China (North Latitude 36°40′). The solar irradiance was calculated based on the standard clear-sky condition [48]. The maximum absorbed daily solar irradiance is about 650 W/m^2 in summer (see Fig. 13(a)). Regarding its hourly variations, it increases from 0 at sunrise to the maximum value at solar noon and then drops to 0 at sunset, as shown in Fig. 13(b). In terms of the ambient air temperature, its daily variations are in accordance with those of the solar irradiance. The difference between the maximum and the minimum daily ambient air temperature is 15 °C (see Fig. 13(c)). Over a typical day, a linear variation of the ambient air temperature was used for simplicity, as shown in Fig. 13(d). It increases from the minimum value at sunrise to the maximum value at 2 pm and drops linearly to the minimum value at sunrise of the next day. The system was supposed to work when the absorbed solar irradiance exceeds 50 W/m^2. In the numerical simulation, this was achieved by controlling the mass flow rate of the circulating water. The adopted time increment for the analysis was 5 mins.

4.1. Transient performance of a typical case

Shown in Fig. 14 are the obtained results for the case of a single energy pile with L = 30 m and D_p = 1.0 m. To make it clear, only results for a few days at intervals of 30 days are shown in the figure. For each day, in accordance with the hourly variations of the solar radiation and the ambient air temperature (see Fig. 13), the inlet and outlet temperature increase first, reach a peak value and then decrease. The maximum inlet temperature gradually increases with time and reaches slightly more than 30 °C after about 210 days of operation. This is due to the continuous solar energy storage in the ground and the resultant gradual increase of the ground temperature, as shown in Fig. 14(b). The curve of the ground temperature distribution along path 1 (see Fig. 3) continues to expand outwards with time. This means a wider zone being thermally influenced and a gradual increase in the ground temperature. After 210 days of solar energy storage, the temperature of the energy pile reaches the maximum value of about 24 °C. The corresponding temperature increase of the pile is about 9 °C, which is within the normal operating temperature range of energy piles ($\Delta T \leq 20$ °C) when

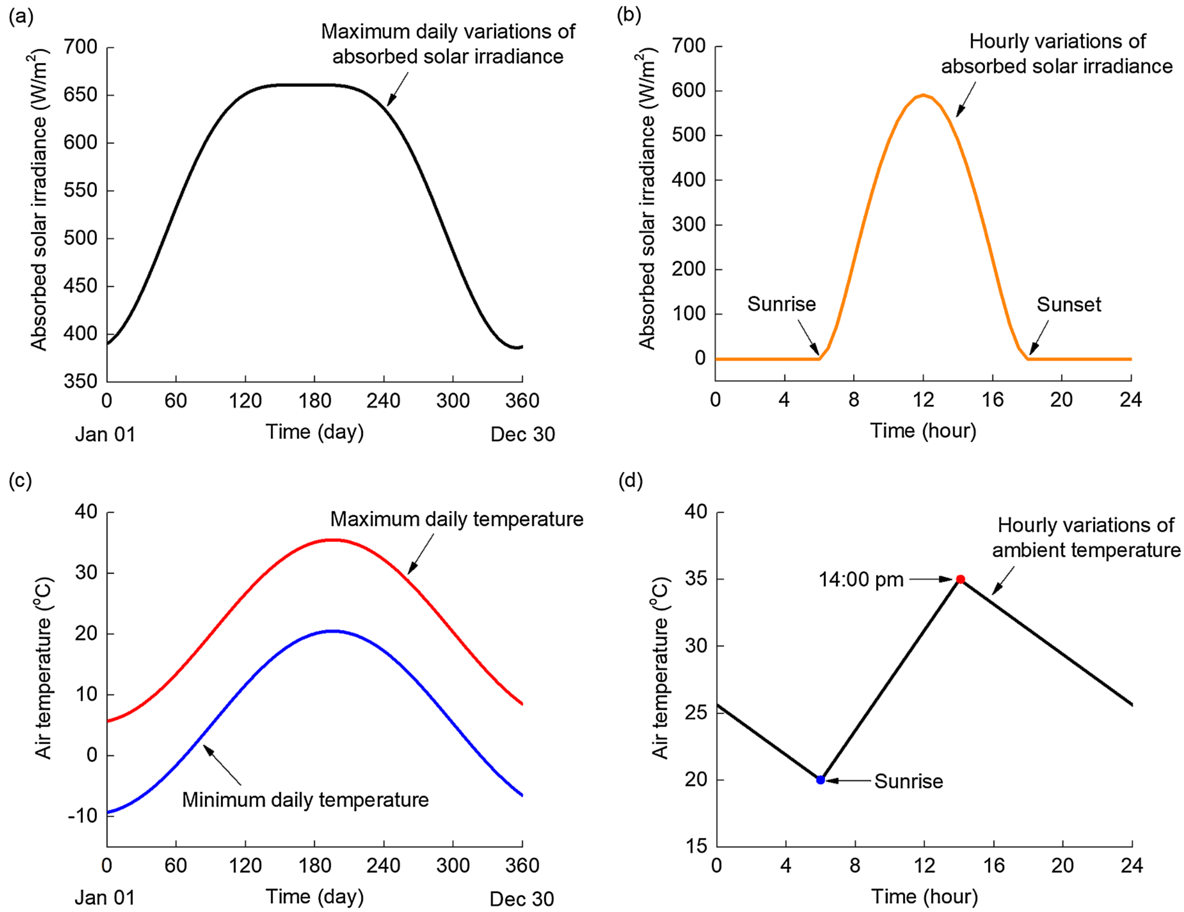

Fig. 13. Adopted daily and hourly variations of the absorbed solar irradiance and the ambient air temperature for the transient-state analysis: (a) maximum daily variations of the absorbed solar irradiance throughout a year; (b) hourly variations of the absorbed solar irradiance over a typical day; (c) maximum and minimum daily variations of the ambient air temperature throughout a year; (d) hourly variations of the ambient air temperature over a typical day.

used for the GSHP system. Afterward, the temperature of the energy pile and the adjacent ground decreases with time, while that of the far-away ground increases. This indicates a transfer of stored solar energy from the ground adjacent to the energy pile to the far-field. This transfer is induced by the gradual decrease in the rate of solar energy storage after about 210 days (see Fig. 14(c)). By the end of the one-year operation, the temperature of the energy pile drops to about 20 °C with an increment of about 5 °C. During the one-year operation, the maximum temperature of the storage system is below 30 °C. Therefore, it can be characterized as a low-temperature system [49], which is advantageous to reduce heat loss due to self-discharge.

The gradual increase of the ground temperature leads to a decrease in the rate of solar energy storage. A higher ground temperature makes it more difficult to further inject heat into the ground due to the reduced temperature gradient between the circulating water and the surrounding ground. As demonstrated in Fig. 14(c), by the end of the one-year operation, both the peak and the average rate of solar energy storage are slightly smaller than the corresponding values at the beginning. The radius of the ground being thermally affected reaches about 10 m (see Fig. 14(b)), which is 10 times the pile diameter. Usually, the pile-pile spacing is about 3–5 times the pile diameter. Therefore, thermal interference between energy piles will occur if installed in a pile group. The rate of solar thermal energy storage is thus expected to decrease more due to an even higher increase in ground temperature for an energy pile group.

4.2. Effects of the pile length

Fig. 15 compares the thermal performance of the single energy pile-solar collector coupled system with three different pile lengths (L = 10 m, 30 m, and 50 m). It can be seen from Fig. 15(a) that as the pile length increases, the daily average inlet temperature decreases. The maximum daily average inlet temperature for the case with L = 10 m is about 10 °C higher than that for the case with L = 50 m. This is due to the higher temperature increase of the pile and the surrounding ground for the shorter energy piles, as shown in Fig. 15(b). As the pile length decreases, the volume of ground for solar energy storage decreases. For the same amount of solar energy storage, the temperature increase is higher for a smaller storage volume. For the case with L = 10 m, the maximum temperature increase of the pile is about 16 °C after 210 days, which is about 10 °C higher than that for the case with L = 50 m. Although the temperature increase is higher for cases with shorter energy piles, the zone being thermally influenced is roughly the same.

As the pile length increases, it allows more time for heat transfer between the circulating water and the energy pile. This results in a larger inlet-outlet temperature difference for the longer energy piles, as shown in Fig. 15(c). The maximum daily average inlet-outlet temperature difference for the case with L = 50 m is about 2 °C higher than that for the case with L = 10 m. This means a higher total solar energy storage rate for the longer energy piles. If the total solar energy storage

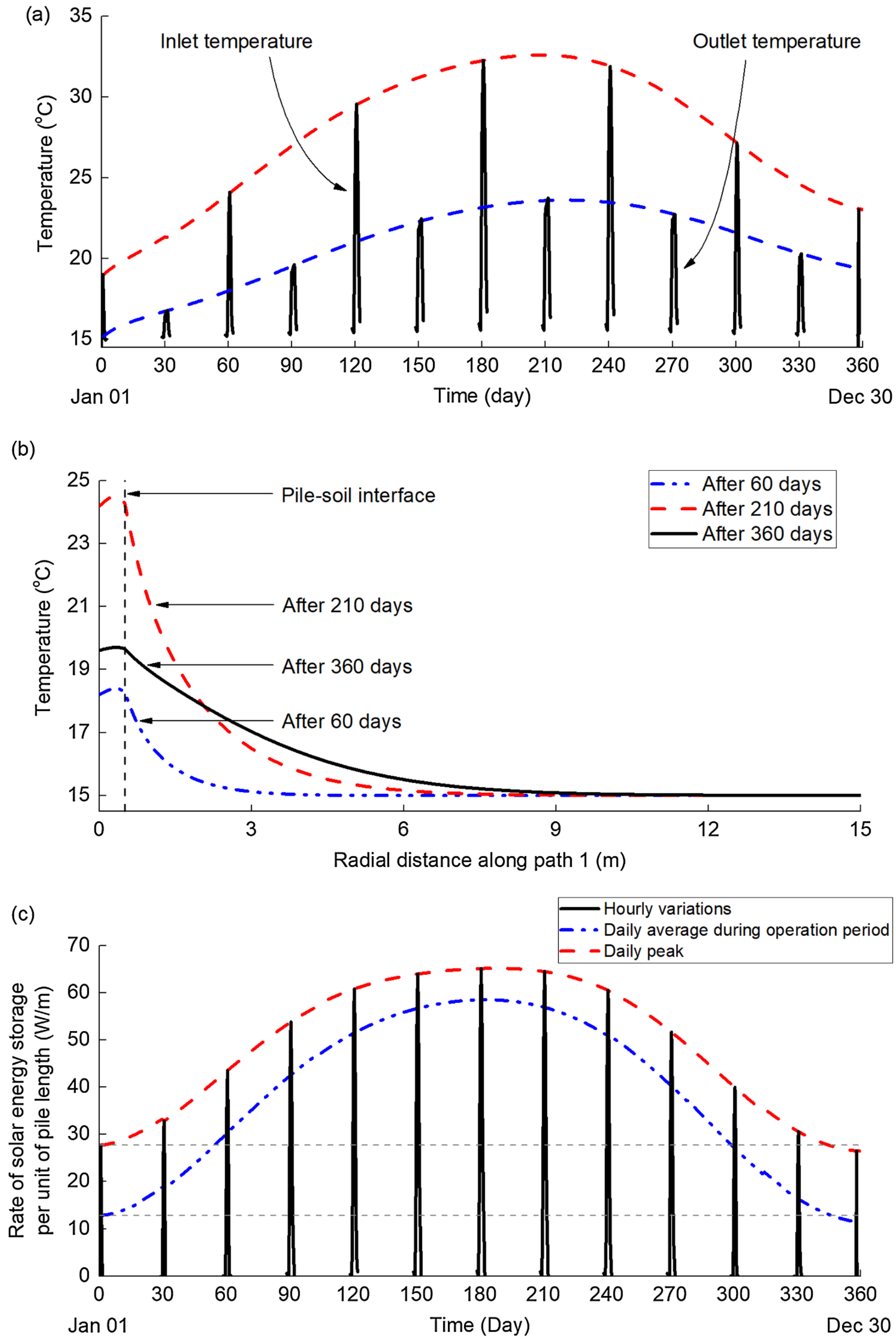

Fig. 14. Evolution with time of: (a) inlet and outlet temperature; (b) distribution of ground temperature along path 1 (vertically halfway the pile length); (c) rate of solar energy storage.

rate is divided by the pile length, however, the shorter energy piles are superior over the longer energy piles (see Fig. 15(d)). The maximum daily average rate of solar energy storage decreases from as high as 150 W/m for the case with $L = 10$ m to about 35 W/m as the pile length increases to 50 m. The maximum daily average rate of solar energy storage for the case with $L = 30$ m is slightly over 50 W/m. To improve its thermal performance, solar collectors with a larger area should be adopted for the longer energy piles. Further study of optimal design is necessary to maximize its thermal performance of underground solar energy storage while ensuring its safety in terms of both deformation and bearing capacity. From an economic point of view, Fig. 15(d) can serve to determine the operation of the system while taking into consideration the cost of the circulation pump. A minimum value of solar energy storage rate can be calculated, below which the operation of solar energy storage should be stopped.

4.3. Effects of the pile diameter

The effects of the pile diameter on the thermal performance of the energy pile-solar collector coupled system are shown in Fig. 16. It can

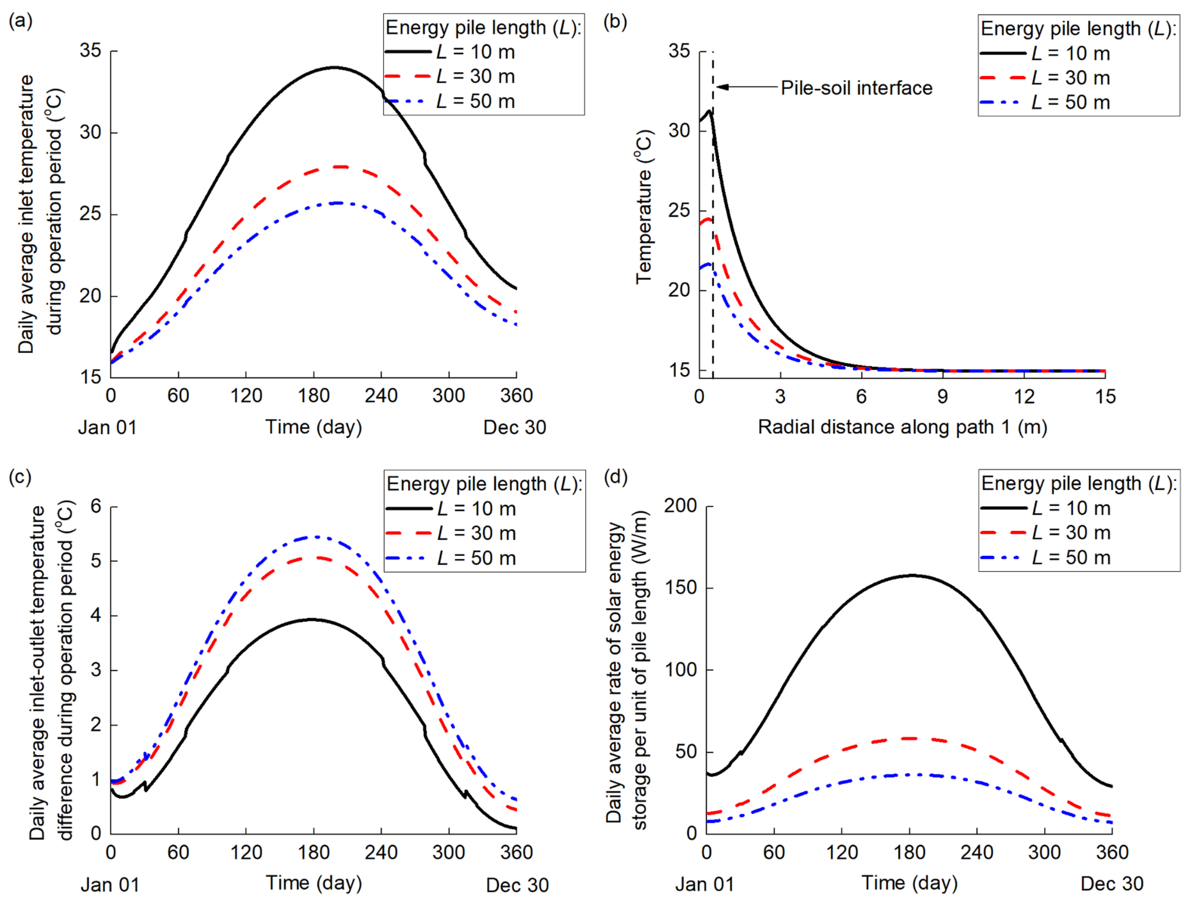

Fig. 15. Comparison of the thermal performance of the system with different pile lengths: (a) daily average inlet temperature during operation period; (b) temperature distribution along path 1 after 210 days (vertically halfway the pile length); (c) daily average inlet-outlet temperature difference during operation period; (d) daily average rate of solar energy storage during operation period.

be seen from Fig. 16(a–b) that both the inlet temperature and the pile temperature are lower for cases with larger pile diameters. The pile temperature for the case with $D_p = 1.5$ m is about 5 °C smaller than that with $D_p = 0.5$ m, which has a maximum pile temperature increase of about 13 °C after 210 days of operation. The density and thermal conductivity of concrete are larger than those of the soil. As the pile diameter increases, there has a relatively larger volume of concrete for solar energy storage, leading to a lower pile temperature. As a result of its lower temperature, a higher rate of solar energy storage is observed for cases with larger pile diameters. As shown in Fig. 16(d), the maximum daily average rate of solar energy storage for the case with $D_p = 1.5$ m is about 5 W/m (10%) larger than that with $D_p = 0.5$ m. In combination with the previous section, it can be concluded that to increase either the pile length or the pile diameter can contribute to maintaining the temperature of the system relatively lower and thus improving the rate of solar energy storage.

4.4. Effects of the pile-pile thermal interference

As shown above, after one year of solar energy storage, the ground being thermally affected had a radius of up to 10 m. Therefore, when installed in a group pile-pile thermal interference is expected. To quantify the effects of the pile-pile thermal interference on the rate of solar energy storage, one 2 × 2 and one 3 × 3 energy pile group were simulated (see Table 2 series 7). The pile-pile spacing was 3 times the pile diameter, which represents the minimum pile spacing for most engineering applications. Therefore, the pile-pile thermal interference is expected to be most noticeable. Fig. 17 compares the daily average rate of solar energy storage for each energy pile of the groups to that of the single energy pile with the same pile length and pile diameter. It shows that initially there is no thermal interference between piles until after about 90 days of solar energy storage. This is because the thermal front generated by each energy pile did not meet each other initially. Afterward, the effects of the pile-pile thermal interference on reducing the rate of solar energy storage appear and gradually increase. As expected, the middle pile of the 3 × 3 group is to suffer most from the pile-pile thermal interference. By the end of the one-year operation, its daily average rate of solar energy storage is about 10 W/m less than that of the single energy pile. In addition, the daily average rate of solar energy storage of the corner pile of the 3 × 3 group is also less than that of the corner pile of the 2 × 2 group. This is due to that the former is thermally affected by more energy piles than the latter, leading to a higher increase in the ground temperature as discussed below.

Shown in Fig. 18 is the temperature distribution across the region surrounding the energy piles with a diameter of about 9 m at three different time points. The case of the single energy pile has been analyzed before (see Fig. 14(b)). For the 2 × 2 and the 3 × 3 group, temperature changes of each energy pile and its adjacent ground are roughly the same at the beginning. This condition exists during the first 90 days of operation and indicates no pile-pile thermal interference, as also confirmed by the results of the solar energy storage rate shown in Fig. 17. As the process of solar energy storage continues, the pile-pile thermal interference occurs, resulting in that the temperature at the center of the pile group gradually increases. By the end of the one-year solar energy storage, the contour of the temperature distribution shows concentric circles centered at the middle point of the group for both the

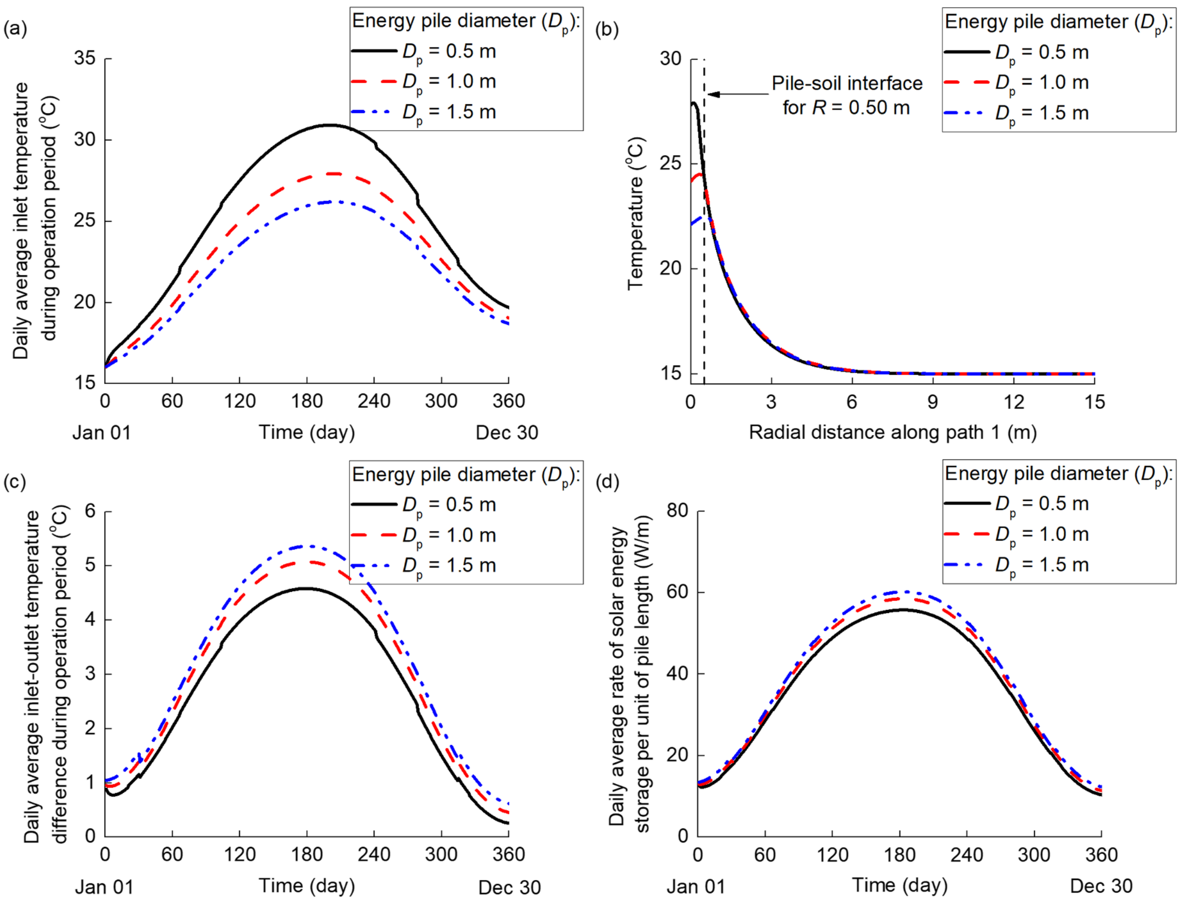

Fig. 16. Comparison of the thermal performance of the system with different pile diameters: (a) daily average inlet temperature during operation period; (b) temperature distribution along path 1 after 210 days (vertically halfway the pile length); (c) daily average inlet-outlet temperature difference during operation period; (d) daily average rate of solar energy storage during operation period.

2 × 2 and the 3 × 3 energy pile group. This indicates a concentration of the stored solar energy within the region of the pile group, being consistent with the analysis results from Başer et al. [43]. By the end of the one-year operation, the maximum temperature for the 2 × 2 and the 3 × 3 energy pile group is about 30 °C and 35 °C, respectively. Both are higher than that of the single energy pile, about 20 °C. This is the reason behind the relatively higher rate of solar energy storage generated by the single energy pile (see Fig. 17).

5. Conclusions

This study evaluated the thermal performance of an energy pile-solar collector coupled system for underground solar energy storage. Both steady-state and transient-state analyses were conducted to quantify the effects of relevant design parameters and the evolution with time of its thermal performance throughout a year. Based on the results and discussions presented, the authors attempt to draw the following conclusions:

1) For the energy pile-solar collector coupled system to store solar energy underground, lower flow rates of the circulating water were preferred to save the operational cost of the circulation pump at only a slight sacrifice of the rate of solar energy storage. For the specific case simulated, the decrease in the rate of solar energy storage was about 2% as the mass flow rate was reduced from 0.3 to 0.05 kg/s.
2) The thermal performance of the system was quite sensitive to the water content of the ground (soil in this study). When the ground turned from being completely dry to being fully saturated, the rate of solar energy storage increased by about 20%.
3) Throughout a year, the rate of solar energy storage changed in accordance with that of the solar irradiance and the ambient air temperature. Under the specific thermal boundary conditions adopted, the maximum daily average rate of solar energy storage reached 150 W/m for the 10 m-long energy pile. It decreased to about 35 W/m as the pile length increased to 50 m. In addition, due to the gradual build-up of the ground temperature, the rate of solar energy storage by the end of the one-year operation was smaller than that at the beginning.
4) It was found that a larger pile size in terms of both the pile diameter and the pile length was favorable to keep system temperature relatively lower, and thus improved the total rate of solar energy storage. This is because the concrete pile material has a relatively larger density and thermal conductivity compared to the soil. This also implies that to increase the density, thermal conductivity, and heat capacity of the pile material can further improve the thermal performance of the energy pile-solar collector coupled system for underground solar energy storage.
5) For the simulated cases, the maximum temperature increase experienced by the energy pile was about 16 °C after a 210-day operation. By the end of the one-year operation, the ground being thermally affected had a radius of about 10 m, indicating potential pile-pile thermal interference. Quantitatively, the effects of the pile-pile thermal interference on reducing the rate of solar energy storage were less than 10 W/m for an energy pile group with pile spacing of 3 times the pile diameter after a one-year operation.

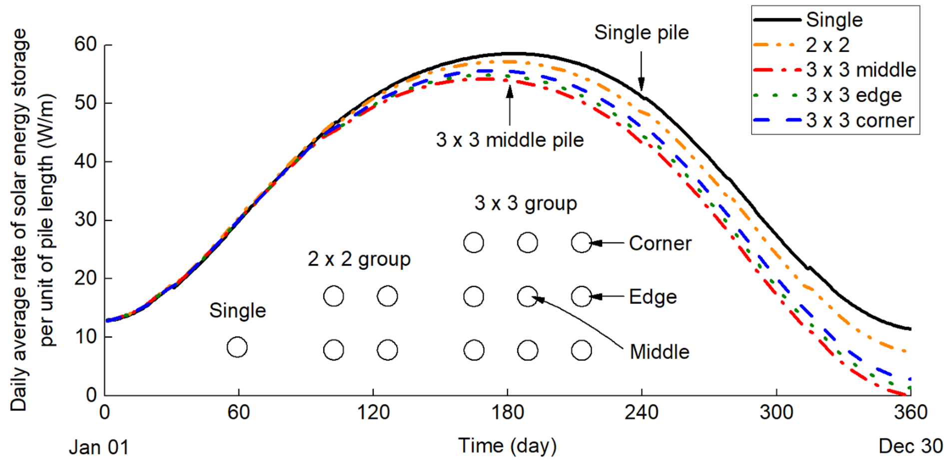

Fig. 17. Effects of the pile-pile thermal interference on the daily average rate of solar energy storage.

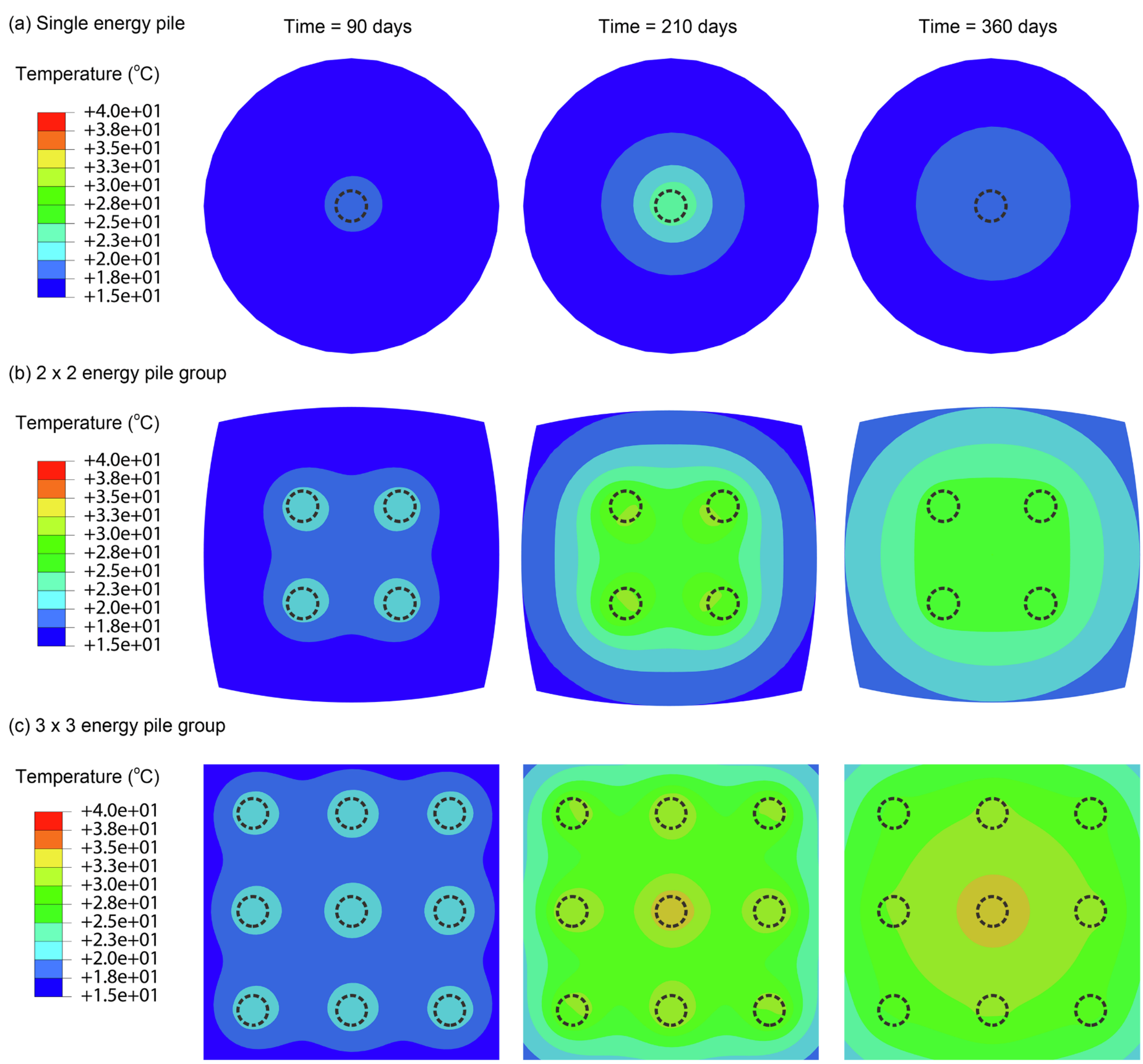

Fig. 18. Evolution of temperature distribution with time for different cases (vertically halfway the pile length): (a) single energy pile; (b) 2 × 2 energy pile group; (c) 3 × 3 energy pile group.

CRediT authorship contribution statement

Qijie Ma: Conceptualization, Methodology, Data curation, Validation, Writing - original draft, Writing - review & editing. **Peijun Wang:** Funding acquisition, Resources, Software, Writing - review & editing.

Declaration of Competing Interest

The authors declared that there is no conflict of interest.

Acknowledgements

This work was supported by the National Natural Science Foundation of China (grant number 51908328).

References

[1] International Energy Agency. World Energy Outlook 2018. Paris: OECD/IEA; 2018.
[2] Yan J, Yang X. Thermal energy storage. Appl Energy 2019;240:A1–6.
[3] Guelpa E, Verda V. Thermal energy storage in district heating and cooling systems: a review. Appl Energy 2019;252:113474.
[4] Pinel P, Cruickshank CA, Beausoleil-Morrison I, Wills A. A review of available methods for seasonal storage of solar thermal energy in residential applications. Renew Sustain Energy Rev 2011;15(7):3341–59.
[5] Xu J, Wang RZ, Li Y. A review of available technologies for seasonal thermal energy storage. Sol Energy 2014;103:610–38.
[6] Gao L, Zhao J, Tang Z. A review on borehole seasonal solar thermal energy storage. Energy Procedia 2015;70:209–18.
[7] Brandl H. Energy foundations and other thermo-active ground structures. Géotechnique 2006;56(2):81–122.
[8] Gao J, Zhang X, Liu J, Li K, Yang J. Numerical and experimental assessment of thermal performance of vertical energy piles: an application. Appl Energy 2008;85(10):901–10.
[9] Sani AK, Singh RM, Amis T, Cavarretta I. A review on the performance of geothermal energy pile foundation, its design process and applications. Renew Sustain Energy Rev 2019;106:54–78.
[10] Batini N, Loria AFR, Conti P, Testi D, Grassi W, Laloui L. Energy and geotechnical behaviour of energy piles for different design solutions. Appl Therm Eng 2015;86:199–213.
[11] Go GH, Lee SR, Yoon S, Kang HB. Design of spiral coil PHC energy pile considering effective borehole thermal resistance and groundwater advection effects. Appl Energy 2014;125:165–78.
[12] Park S, Lee D, Lee S, Chauchois A, Choi H. Experimental and numerical analysis on thermal performance of large-diameter cast-in-place energy pile constructed in soft ground. Energy 2017;118:297–311.
[13] Guo Y, Zhang G, Liu S. Investigation on the thermal response of full-scale PHC energy pile and ground temperature in multi-layer strata. Appl Therm Eng 2018;143:836–48.
[14] Zhao Q, Chen B, Liu F. Study on the thermal performance of several types of energy pile ground heat exchangers: U-shaped, W-shaped and spiral-shaped. Energy Build 2016;133:335–44.
[15] Park S, Lee S, Lee D, Ahn D, Choi H. Effect of thermal interference on energy piles considering various configurations of heat exchangers. Energy Build 2019;199:381–401.
[16] Huang G, Yang X, Liu Y, Zhuang C, Zhang H, Lu J. A novel truncated cone helix energy pile: modelling and investigations of thermal performance. Energy Build 2018;158:1241–56.
[17] Liu Y, Huang G, Lu J, Yang X, Zhuang C. A novel truncated cone helix energy pile: numerical and laboratory investigations of thermal performance. Int J Heat Mass Transf 2018;126:681–99.
[18] Faizal M, Bouazza A, Singh RM. Heat transfer enhancement of geothermal energy piles. Renew Sustain Energy Rev 2016;57:16–33.
[19] Li M, Lai ACK. Review of analytical models for heat transfer by vertical ground heat exchangers (GHEs): a perspective of time and space scales. Appl Energy 2015;151:178–91.
[20] Liu H, Maghoul P, Bahari A, Kavgic M. Feasibility study of snow melting system for bridge decks using geothermal energy piles integrated with heat pump in Canada. Renewable Energy 2019;136:1266–80.
[21] Kong G, Wu D, Liu H, Laloui L, Cheng X, Zhu X. Performance of a geothermal energy deicing system for bridge deck using a pile heat exchanger. Int J Energy Res 2019;43:596–603.
[22] Wood CJ, Liu H, Riffat SB. An investigation of the heat pump performance and ground temperature of a piled foundation heat exchanger system for a residential building. Energy 2010;35(12):4932–40.
[23] You T, Li X, Cao S, Yang H. Soil thermal imbalance of ground source heat pump systems with spiral-coil energy pile groups under seepage conditions and various influential factors. Energy Convers Manage 2018;178:123–36.
[24] Akrouch GA, Sánchez M, Briaud JL. Thermal performance and economic study of an energy piles system under cooling dominated conditions. Renewable Energy 2018.
[25] Shah SK, Aye L, Rismanchi B. Seasonal thermal energy storage system for cold climate zones: A review of recent developments. Renew Sustain Energy Rev 2018;97:38–49.
[26] Welsch B, Göllner-Völker L, Schulte DO, Bär K, Sass I, Schebek L. Environmental and economic assessment of borehole thermal energy storage in district heating systems. Appl Energy 2018;216:73–90.
[27] Yang H, Cui P, Fang Z. Vertical-borehole ground-coupled heat pumps: a review of models and systems. Appl Energy 2010;87(1):16–27.
[28] Rad FM, Fung AS, Leong WH. Feasibility of combined solar thermal and ground source heat pump systems in cold climate, Canada. Energy Build 2013;61:224–32.
[29] Mesquita L, McClenahan D, Thornton J, Carriere J, Wong B Drake. Landing Solar Community: 10 years of operation. ISES Solar World Congress 2017.
[30] Ng CWW, Ma QJ, Gunawan A. Horizontal stress change of energy piles subjected to thermal cycles in sand. Comput Geotech 2016;78:54–61.
[31] Ng CWW, Ma QJ. Energy pile group subjected to non-symmetrical cyclic thermal loading in centrifuge. Géotechnique Letters 2019;3:1–5.
[32] Duffie JA, Beckman WA. Solar engineering of thermal processes. 2nd ed. New York: Wiley Interscience; 1991.
[33] McDaniel B, Kosanovic D. Modeling of combined heat and power plant performance with seasonal thermal energy storage. J Storage Mater 2016;7:13–23.
[34] Li C, Mao J, Xing Z, Zhou J, Li Y. Analysis of geo-temperature restoration performance under intermittent operation of borehole heat exchanger fields. Sustainability 2016;8(1):35.
[35] Johansen O. Thermal conductivity of soils. PhD thesis, University of Trondheim, CRREL Draft English Translation 637; 1977.
[36] Choi JC, Lee SR, Lee DS. Numerical simulation of vertical ground heat exchangers: intermittent operation in unsaturated soil conditions. Comput Geotech 2011;38(8):949–58.
[37] EN 1992-1-2 (2004) European Committee for Standardization (CEN). Design of concrete structures—Part 1-2: General rules—Structural fire design. EN 1992 Eurocode 2; 2004.
[38] Park H, Lee SR, Yoon S, Choi JC. Evaluation of thermal response and performance of PHC energy pile: Field experiments and numerical simulation. Appl Energy 2013;103:12–24.
[39] ABAQUS Inc. ABAQUS user's manual Ver. 6.13. Rhode Island 2013.
[40] Bozis D, Papakostas K, Kyriakis N. On the evaluation of design parameters effects on the heat transfer efficiency of energy piles. Energy Build 2011;43(4):1020–9.
[41] Bourne-Webb PJ, Bodas Freitas TM, Freitas Assunção RM. Soil–pile thermal interactions in energy foundations. Géotechnique 2015;66(2):167–71.
[42] Sani AK, Singh RM. Response of unsaturated soils to heating of geothermal energy pile, Renewable Energy, https://doi.org/10.1016/j.renene.2018.11.032.
[43] Başer T, Lu N, McCartney JS. Operational response of a soil-borehole thermal energy storage system. J Geotech Geoenviron Eng 2015;142(4):04015097.
[44] Miyara A, Tsubaki K, Inoue S, Yoshida K. Experimental study of several types of ground heat exchanger using a steel pile foundation. Renewable Energy 2011;36(2):764–71.
[45] Park S, Lee S, Oh K, Kim D, Choi H. Engineering chart for thermal performance of cast-in-place energy pile considering thermal resistance. Appl Therm Eng 2018;130:899–921.
[46] Zarrella A, De Carli M, Galgaro A. Thermal performance of two types of energy foundation pile: helical pipe and triple U-tube. Appl Therm Eng 2013;61(2):301–10.
[47] Akrouch GA, Sánchez M, Briaud JL. An experimental, analytical and numerical study on the thermal efficiency of energy piles in unsaturated soils. Comput Geotech 2016;71:207–20.
[48] Hottel HC. A simple model for estimating the transmittance of direct solar radiation through clear atmospheres. Sol Energy 1976;18(2):129–34.
[49] Hesaraki A, Holmberg S, Haghighat F. Seasonal thermal energy storage with heat pumps and low temperatures in building projects—A comparative review. Renew Sustain Energy Rev 2015;43:1199–213.